

10  
I29A  
568  
C.2

# **CIVIL ENGINEERING STUDIES**

STRUCTURAL RESEARCH SERIES NO. 568

UILU-ENG-92-2005



ISSN: 0069-4274

## **THE INFLUENCE OF WELD STRENGTH MISMATCH ON CRACK-TIP CONSTRAINT IN SINGLE EDGE NOTCH BEND SPECIMENS**

By  
MARK T. KIRK  
ROBERT H. DODDS, JR.

A Report on a Research Project  
Sponsored by the  
DAVID TAYLOR RESEARCH CENTER  
METALS AND WELDING DIVISION  
ANNAPOLIS, MARYLAND

DEPARTMENT OF CIVIL ENGINEERING  
UNIVERSITY OF ILLINOIS AT  
URBANA-CHAMPAIGN  
URBANA, ILLINOIS  
FEBRUARY 1992

# **The Influence of Weld Strength Mismatch on Crack–Tip Constraint in Single Edge Notch Bend Specimens**

By

Mark T. Kirk

Robert H. Dodds, Jr.

*Department of Civil Engineering*

*University of Illinois*

*A Report on a Research Project Sponsored by the:*

**DAVID TAYLOR RESEARCH CENTER**

**METALS AND WELDING DIVISION**

*Annapolis, Maryland 21402*

University of Illinois

Urbana, Illinois

February 1992

<b>REPORT DOCUMENTATION PAGE</b>	<b>1. REPORT NO.</b> UILU-ENG-92-2005	<b>2.</b>	<b>3. Recipient's Accession No.</b>
<b>4. Title and Subtitle</b> The Influence of Weld Strength Mismatch on Crack-Tip Constraint in Single Edge Notch Bend Specimens		<b>5. Report Date</b> February 1992	
		<b>6.</b>	
<b>7. Author(s)</b> Mark T. Kirk and Robert H. Dodds, Jr.		<b>8. Performing Organization Report No.</b> SRS-568	
<b>9. Performing Organization Name and Address</b> University of Illinois at Urbana-Champaign Department of Civil Engineering 205 N. Mathews Avenue Urbana, Illinois 61801		<b>10. Project/Task/Work Unit No.</b>	
		<b>11. Contract(C) or Grant(G) No.</b> N61533-90-K-0059	
<b>12. Sponsoring Organization Name and Address</b> David Taylor Research Center Metal and Welding Division, Code 281 Annapolis, Maryland 21402		<b>13. Type of Report &amp; Period Covered</b> Interim: 1-1-91 to 1-1-92	
		<b>14.</b>	
<b>15. Supplementary Notes</b>			
<b>16. Abstract (Limit: 200 words)</b> <p>Dodds and Anderson provide a framework to quantify finite size and crack depth effects on fracture toughness when failure occurs at deformation levels where <math>J</math> no longer uniquely describes the state of stresses and strains in the vicinity of the crack-tip. Size effects on cleavage fracture are quantified by defining a value termed <math>J_{SSY}</math>: the <math>J</math> to which an infinite body must be loaded to achieve the same stressed volume, and thereby the same likelihood of cleavage fracture, as in a finite body. In weld metal fracture toughness testing, mismatch between weld metal and baseplate strength can alter deformation patterns, which complicates size and crack depth effects on cleavage fracture toughness. However, the virtually limitless number of weld joint geometry / crack depth combinations preclude calculation of <math>J_{SSY}</math> for each individual case. This study addresses the accuracy with which <math>J_{SSY}</math> for a welded single edge notch bend, SE(B), specimen can be approximated by previously published results for homogeneous specimens. The case of a crack located on the weld joint centerline is treated. The combined effects of weld groove type, degree of mismatch, and crack depth to specimen width (<math>a/W</math>) ratio are considered by performing plane-strain elastic-plastic finite element analyses of SE(B) specimens containing a variety of common weld groove details. These results demonstrate virtually no effect of <math>\pm 20\%</math> mismatch on <math>J_{SSY}</math> if the distance from the crack-tip to the weld/plate interface (<math>L_{min}</math>) exceeds 0.2-inches. If <math>L_{min}</math> falls below 0.2-inches, there exists a deformation (applied-<math>J</math>) dependent value of <math>L_{min}</math> below which reasonably accurate <math>J_{SSY}</math> estimation is possible. At higher levels of overmatch (50% to 100%), it is no longer possible to parameterize departure of <math>J_{SSY}</math> for a weldment from that for a homogeneous SE(B) based on <math>L_{min}</math> alone. Weld geometry significantly influences the accuracy with which <math>J_{SSY}</math> for a welded SE(B) can be approximated by <math>J_{SSY}</math> for a homogeneous specimen at these extreme overmatch levels.</p>			
<b>17. Document Analysis    a. Descriptors</b> <p>Constraint effects, <math>J_{SSY}</math> estimation, Fracture mechanics, Finite elements, Weld strength mismatch</p> <p><b>b. Identifiers/Open-Ended Terms</b></p> <p><b>c. COSATI Field/Group</b></p>			
<b>18. Availability Statement</b>  Release Unlimited	<b>19. Security Class (This Report)</b> UNCLASSIFIED		<b>21. No. of Pages</b> 23
	<b>20. Security Class (This Page)</b> UNCLASSIFIED		<b>22. Price</b>

# ABSTRACT

Dodds and Anderson provide a framework to quantify finite size and crack depth effects on fracture toughness when failure occurs at deformation levels where  $J$  no longer uniquely describes the state of stresses and strains in the vicinity of the crack—tip. Size effects on cleavage fracture are quantified by defining a value termed  $J_{SSY}$ : the  $J$  to which an infinite body must be loaded to achieve the same stressed volume, and thereby the same likelihood of cleavage fracture, as in a finite body. In weld metal fracture toughness testing, mismatch between weld metal and baseplate strength can alter deformation patterns, which complicates size and crack depth effects on cleavage fracture toughness. However, the virtually limitless number of weld joint geometry / crack depth combinations preclude calculation of  $J_{SSY}$  for each individual case. This study addresses the accuracy with which  $J_{SSY}$  for a welded single edge notch bend, SE(B), specimen can be approximated by previously published results for homogeneous specimens. The case of a crack located on the weld joint centerline is treated. The combined effects of weld groove type, degree of mismatch, and crack depth to specimen width ( $a/W$ ) ratio are considered by performing plane—strain elastic—plastic finite element analyses of SE(B) specimens containing a variety of common weld groove details. These results demonstrate virtually no effect of  $\pm 20\%$  mismatch on  $J_{SSY}$  if the distance from the crack—tip to the weld/plate interface ( $L_{min}$ ) exceeds 0.2— inches. If  $L_{min}$  falls below 0.2— inches, there exists a deformation (applied— $J$ ) dependent value of  $L_{min}$  below which reasonably accurate  $J_{SSY}$  estimation is possible. At higher levels of overmatch (50% to 100%), it is no longer possible to parameterize departure of  $J_{SSY}$  for a weldment from that for a homogeneous SE(B) based on  $L_{min}$  alone. Weld geometry significantly influences the accuracy with which  $J_{SSY}$  for a welded SE(B) can be approximated by  $J_{SSY}$  for a homogeneous specimen at these extreme overmatch levels.

## ACKNOWLEDGMENTS

This report was prepared as part of the Surface Ship and Submarine Materials Block under the sponsorship of I. L. Caplan (David Taylor Research Center (DTRC), Code 011.5). The work supports DTRC Program Element 62234N, Task Area RS345S50. The work of the first author was conducted at the University of Illinois as part of a training program administered by DTRC. Support for R.H. Dodds was provided by DTRC under contract number N61533-90-K-0059. Computational support and reproduction of this report were made possible by DTRC Contract No. N61533-90-K-0059.

# TABLE OF CONTENTS

Section No.	Page
<b>1. Introduction</b> .....	1
<b>2. Micromechanical Constraint Corrections</b> .....	2
2.1 Crack–Tip Stresses in Infinite Bodies .....	3
2.2 Crack–Tip Stresses in Finite Bodies .....	4
2.3 Calculation of Constraint Corrections .....	5
2.3.1 Use of Crack Plane Stresses to Define $J_{SSY}$ .....	6
2.3.2 Use of Stressed Areas to Define $J_{SSY}$ .....	8
2.3.3 Comparison of these Techniques .....	10
<b>3. Approach</b> .....	12
<b>4. Finite Element Modelling</b> .....	13
<b>5. Results and Discussion</b> .....	15
5.1 Finite Element Results for $\pm 20\%$ Mismatch .....	15
5.2 Justification of Assumptions in Approach .....	17
5.2.1 HAZ Modelling .....	17
5.2.2 Effect of Constitutive Properties .....	20
5.2.3 Effect of Extreme Overmatch .....	21
<b>6. Summary and Conclusions</b> .....	22
<b>7. References</b> .....	22

# LIST OF TABLES

Table No.		Page
1	Fit Coefficients for eqn. 2.3.1.1. ....	8
2	Fit Coefficients for eqn. 2.3.2.1. ....	11
3	Constitutive properties for weldment analysis. ....	13
4	Constitutive properties for weldment analysis. ....	20

# LIST OF FIGURES

Figure No.	Page
1 Small scale yield (SSY) model. ....	3
2 Comparison of opening mode stress on the crack plane from the HRR and SSY solutions. ....	4
3 Comparison of maximum principal stress contours for the SSY solution and for an $a/W=0.15$ $n=10$ SE(B). ....	5
4 Conceptual variation of $J_{SSY}$ with $J$ for two different finite bodies. ....	6
5 Variation of maximum principal stress on the crack plane with distance from the crack-tip and applied $-J$ for an $a/W=0.15$ $n=10$ SE(B). ....	7
6 Dependence of $J_{SSY}$ on critical distance ( $r/CTOD$ ) and applied $-J$ for an $a/W=0.15$ $n=10$ SE(B). ....	8
7 Variation of area within a principal stress contour with contour value and applied $-J$ for an $a/W=0.15$ $n=10$ SE(B). ....	9
8 Dependence of $J_{SSY}$ on critical stress ( $\sigma_1/\sigma_o$ ) and applied $-J$ within the limits of principal stress contour validity for an $a/W=0.15$ $n=10$ SE(B). ....	10
9 Comparison of $J_{SSY}$ values determined using the crack line stress and stressed area techniques for an $a/W=0.15$ $n=10$ SE(B). ....	11
10 Weldment geometries analyzed. ....	12
11 Finite element model of a SE(B) specimen containing an $a/W = 0.15$ crack in a single bevel joint. ....	14
12 Constraint correction curves for two $\pm 20\%$ mismatched welds containing $a/W=0.15$ cracks. ....	15
13 Variation of $J_{SSY}$ estimation error with applied $-J$ for $\pm 20\%$ mismatched welds. ....	16
14 Variation of $J_{SSY}$ estimation error at two fixed applied $-J$ levels with minimum distance from the crack-tip to the weld/plate interface for $\pm 20\%$ mismatched welds. ....	17
15 Determination of distance needed from the crack-tip to the weld/plate interface to keep $J_{SSY}$ estimation error below 10% for $\pm 20\%$ mismatched welds. ....	17



16	Effect of applied $-J$ on distance needed from the crack–tip to the weld/plate interface to keep $J_{SSY}$ estimation error below 10% for $\pm 20\%$ mismatched welds. ....	18
17	Finite element mesh detail and yield properties for 0.16 $W$ square groove HAZ model. ...	18
18	Effect of HAZ modelling on the constraint correction curve for the 0.32 $W$ square groove weld. ....	19
19	Effect of HAZ modelling on the constraint correction curve for the 0.16 $W$ square groove weld. ....	19
20	Effect of constitutive properties on $J_{SSY}$ estimation errors for two welds containing $a/W=0.15$ cracks. ....	20
21	Effect of extreme overmatch on $J_{SSY}$ estimation errors for three welds containing $a/W=0.15$ cracks. ....	21

# 1. INTRODUCTION

The application of conventional fracture mechanics to assess the integrity of a cracked structure relies on the notion that a single parameter uniquely characterizes material resistance to fracture. Material resistance to catastrophic brittle fracture is characterized by a critical value of the stress intensity factor,  $K_{Ic}$ , while resistance to the onset of ductile, or upper-shelf, fracture is characterized by a critical value of the  $J$ -integral,  $J_{Ic}$ . Testing standards which govern the measurement of  $K_{Ic}$  and  $J_{Ic}$ , ASTM E399 and ASTM E813 respectively, require sufficient specimen thickness to insure predominantly plane strain conditions at the crack tip and sufficient crack depth to position the crack-tip in a highly constrained bending field. These restrictions are designed to insure the existence of severe conditions for fracture as described by the Hutchinson-Rice-Rosengren (HRR) asymptotic fields [1,2]. The testing standards thereby guarantee that  $K_{Ic}$  and  $J_{Ic}$  are lower-bound, geometry independent measures of fracture toughness. However, cracks in civil and marine structures are seldom this highly constrained, which makes predictions of the fracture resistance of a structure based on laboratory fracture toughness values overly pessimistic.

The British Standards Institute (BSI) has long advocated a more pragmatic, engineering approach to assess the fracture integrity of cracked structures. This approach requires that constraint in the test specimen approximate that of the structure to provide an “appropriate” toughness for use in a structural analysis. The appropriate constraint is achieved by matching thickness and crack depth between specimen and structure. Experimental studies by Sumpter [3] and by Kirk and Dodds [4], comparing cleavage fracture toughness ( $J_c$ ) values of shallow crack bend specimens to  $J_c$  values for part-through semi-elliptical surface cracks, demonstrate the validity of this approach. These studies show that use of geometry dependent fracture toughness values allows more accurate prediction of the fracture performance of structures than is possible using more traditional approaches. However, the task of characterizing fracture toughness becomes more complex as non-standard specimens are required, and different fracture toughness data are needed for each geometry of interest. Further, this approach cannot be economically applied to thick section structures (e.g. nuclear pressure vessels).

While the BSI approach is a useful and frequently applied engineering tool, it fosters the erroneous impression that, even for homogeneous materials, absolute crack depth ( $a$ ), relative crack depth ( $a/W$ ), and thickness ( $B$ ) all influence fracture toughness<sup>1</sup>. These observed size effects on  $J_c$  [5,6] indicate that a single parameter no longer uniquely describes conditions near the crack tip. The increase of  $J_c$  values in shallow crack specimens develops when the in-plane plastic deformation produced by gross bending of the specimen impinges on the local crack tip fields. This relaxes the kinematic constraint against further plastic flow. Once the global and local plastic fields interact, the crack-tip stresses and strains no longer increase in proportion to one another with amplitude governed by  $J$  alone. In this situation, equivalence of  $J$  between specimens of different crack depths does not insure

1. Hereafter the apparent effect of these geometric parameters on fracture toughness are referred to collectively as *size effects*.

the same crack–tip stress and strain fields<sup>2</sup>. As fracture by any micro–mechanism ultimately requires attainment of some critical condition described in terms of stress and/or strain, different values of applied  $J$  and CTOD may be required to achieve these critical conditions in different structures. Thus, the observed crack depth dependence of  $J_c$  is actually an effect on the relation between macroscopic fracture parameters and micro–scale crack driving force.

The distinction between the fictitious finite size effect on fracture toughness and the actual finite size effect on micro–scale crack driving force is unimportant to the practitioner so long as the effect is consistently treated and fracture toughness experiments are available at the “appropriate” constraint level. However, recognizing that finite size influences driving force rather than toughness suggests that the effect can be quantified analytically. Dodds and Anderson demonstrated that combining detailed knowledge of stresses near the crack tip (determined by finite–element analysis) with a micro–mechanics model appropriate for cleavage fracture permits quantification of finite size effects on micro–scale / macro–scale crack driving force relations. Application of these techniques has resolved the apparent size dependencies exhibited in  $J_c$  data from both bending [6–7] and tension [8] experiments. These techniques are discussed in detail in Section 2.

In welded construction, fracture is most likely to occur either in or near the weld as this location contains the most severe residual stresses, potential welding defects, and the lowest fracture toughness. Structural integrity assessments are therefore often based on toughness data derived by testing fracture specimens containing welds. Mismatch between weld metal and baseplate strength can alter the deformation patterns in such specimens, which complicates finite size effects on cleavage fracture toughness. This study addresses the effect of weld strength mismatch on size effects in SE(B) specimens quantified using the techniques developed by Dodds and Anderson. A crack located in the weld metal on the weldment centerline is treated in detail. The combined effects of weld groove type, degree of mismatch, and crack depth to specimen width ( $a/W$ ) ratio are considered.

## 2. MICROMECHANICAL CONSTRAINT CORRECTIONS

Dodds and Anderson [7,9] show that, by quantifying the effects of finite size on micro–scale / macro–scale crack driving force relations, the apparent size effect on fracture toughness can be rigorously predicted without resort to empirical arguments. These size effects become steadily more pronounced as load increases due to the deviation of crack–tip region deformations from the small scale yielding conditions essential for single parameter fracture mechanics (SPFM) to apply. Once SPFM becomes invalid, a micro–mechanics failure criteria is required to establish the the geometry invariant conditions at fracture. Finite–element analysis provides a means to quantify the geometry dependent relations between these conditions and macro–scale crack driving force. This permits (in principle) prediction of fracture in any body from toughness values measured using standard specimens.

2. Similar arguments apply to specimens of differing thickness.

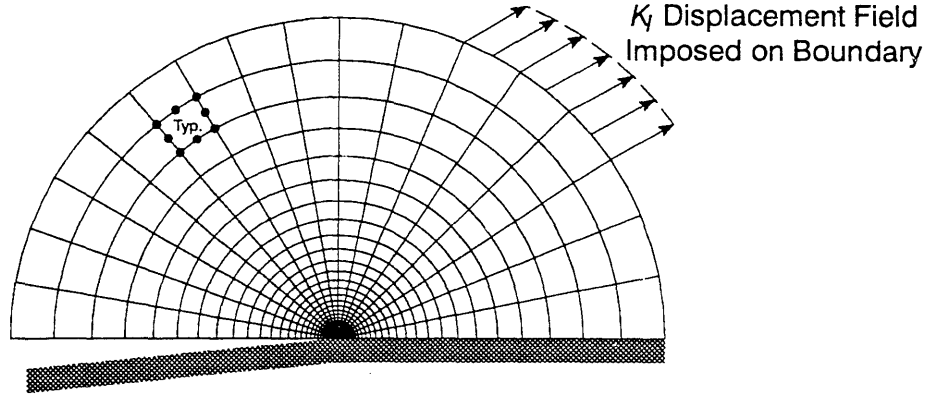


Figure 1: Small scale yield (SSY) model.

For steels operating at temperatures where cleavage occurs after significant plastic deformation but before the initiation of ductile growth (lower to mid-transition), attainment of a critical stress over a microstructurally relevant volume is an appropriate micro-mechanical failure criteria [4]. A number of important engineering structures can fail by this mechanism, including high strength rails, offshore oil platforms, ships, storage tanks, and nuclear pressure vessels after years of neutron irradiation embrittlement. Techniques for predicting the apparent size effects on cleavage fracture toughness developed by Dodds and Anderson are described in the following sections.

## 2.1 Crack-Tip Stresses in Infinite Bodies

An infinite body solution provides the idealized reference needed to quantify the effect of finite size on the crack tip stress state. In classical nonlinear fracture mechanics, the HRR field equations [1–2] serve as this reference solution. However, analysis of the small-scale yielding (SSY) problem demonstrates that the HRR solution does not accurately describe the stress state around a crack tip over the length scale needed to characterize cleavage fracture initiation [7]. The SSY model (Figure 1), originally proposed by Rice and Tracy [11] and McMeeking [12], consists of a circular region containing an edge crack. Boundary displacements are applied to this region consistent with the linear elastic solution for a Mode I crack in an infinite body. Finite element modelling of SSY permits definition of the *full field* solution for a crack in an infinite body over distances of 2 to 10 times the *CTOD*. Steady state conditions are achieved wherein stresses and strains at all angles scale with  $r/(J/\sigma_o)$  and  $r/CTOD$ , as do the HRR fields. This steady state condition persists until the plastic zone size becomes a significant portion of the modelled domain radius,  $\approx 5\%$ , at which point the small-scale yield conditions are violated. The difference between the HRR and SSY solutions for a power law hardening material with a Ramberg–Osgood strain hardening coefficient ( $n$ ) of 10 is shown in Figure 2. While both solutions converge as  $r/CTOD \rightarrow 0$ , demonstrating the asymptotic nature of the HRR solution, the HRR solution becomes inaccurate at distances  $r/CTOD \geq 1$ .

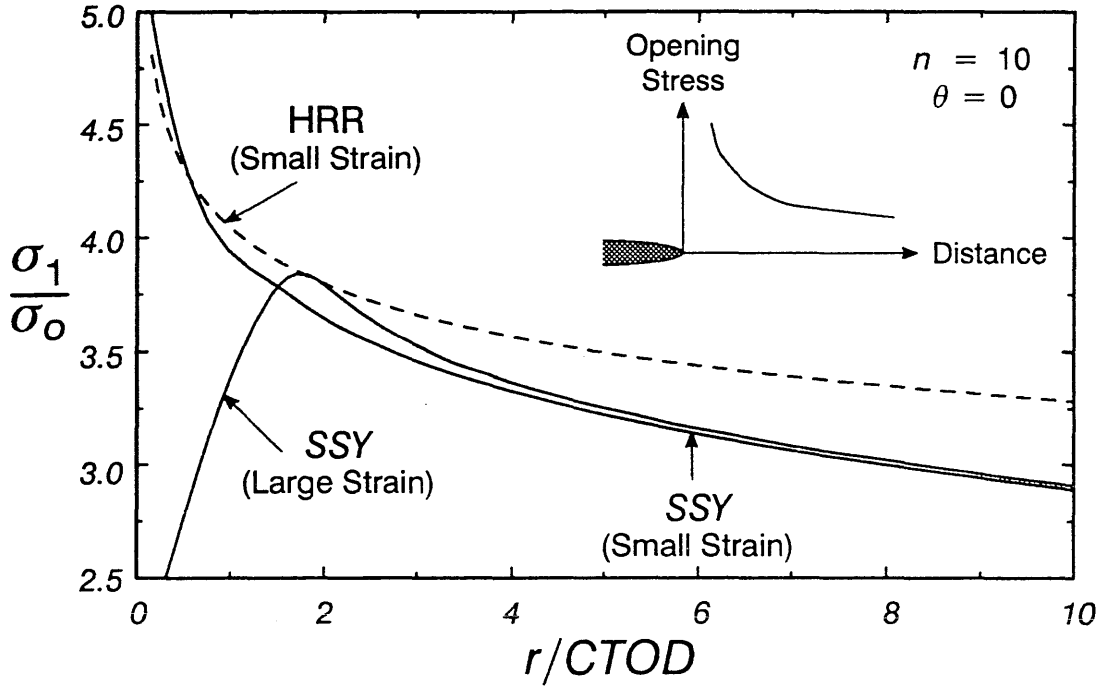


Figure 2: Comparison of opening mode stress on the crack plane from the HRR and SSY solutions.

Both the HRR and SSY solutions are based on conventional small strain theory. Therefore, neither solution models accurately stresses very close to the crack tip where finite blunting deformations, not accounted for within small strain theory, reduce stress. SSY computations employing a finite strain formulation show this reduction at distances  $r/CTOD \leq 2$  [13]. As illustrated in Figure 2, the finite strain and small strain calculations are in very close agreement beyond  $r/CTOD=2$ . These observations indicate that cleavage fracture initiation is unlikely within the zone where finite strain effects dominate due to loss of stress triaxiality, a conclusion supported by experimental observations [14–15]. Thus, the stress distribution defined by the SSY model using conventional small strain theory provides an appropriate reference solution to quantify size effects on crack–tip stress fields. In practice, the SSY stress distribution is defined for the material of interest by finite element analysis for comparison with the stress distribution of the finite body.

## 2.2 Crack–Tip Stresses in Finite Bodies

The distribution of stresses in the crack–tip region of a finite body depends on the geometry, on the mode and magnitude of loading, and on the material strain hardening exponent. Finite element analyses for the situation of interest provide stresses in the crack–tip region for comparison with the SSY reference solution. Stresses are calculated and stored at each load step as the body is deformed toward a limit state. Sufficient mesh refinement is needed to fully define the stresses over distances of 2–10 times the CTOD at all load levels. Such analyses require a considerably more detailed mesh than does a routine analysis to determine  $J$ .

### 2.3 Calculation of Constraint Corrections

Maximum principal stress contours for the SSY problem are compared to those of an  $a/W=0.15, n=10$  single edge notch bend, SE(B), specimen in Figure 3. The finite body effect reduces the peak stress amplitude with increasing deformation. The normalized size of the stressed contour shrinks relative to the SSY limit, which reduces the likelihood of cleavage fracture. However, the spatial distribution

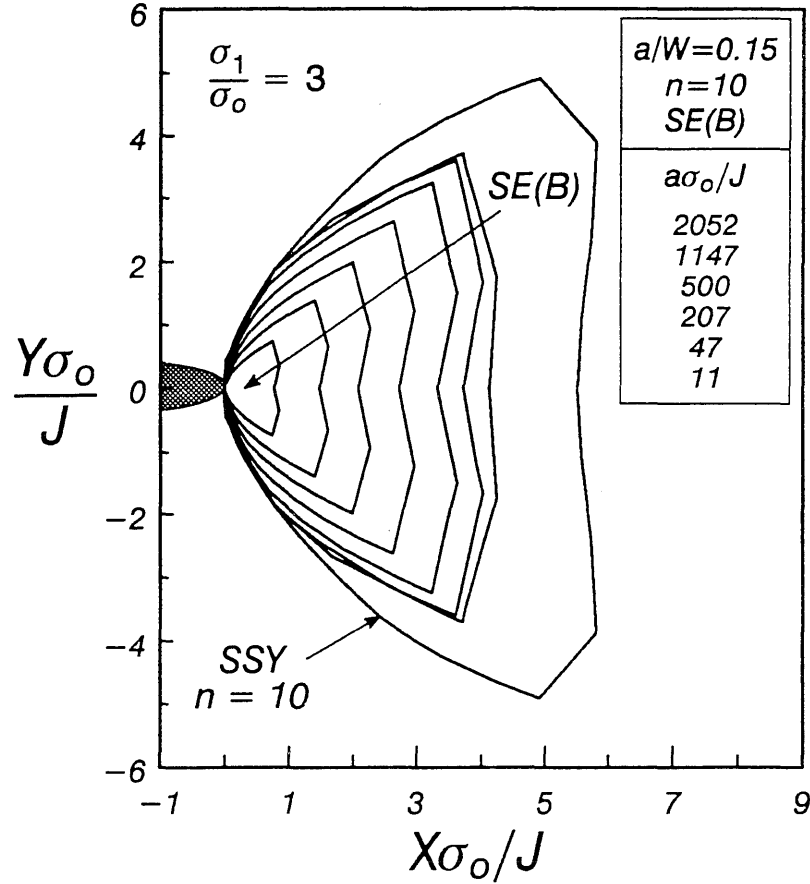


Figure 3: Comparison of a maximum principal stress contour in SSY with those from an  $a/W=0.15, n=10$  SE(B). SE(B) contours decrease in size with increasing deformation (i.e. with decreasing  $a\sigma_0/J$ ).

around the crack is nearly identical in the infinite body and in the finite body, as evidenced by the similarity of the contour shapes. This self-similarity indicates that stressed volumes in infinite and finite bodies differ only by a deformation dependent scalar multiple. The information depicted graphically in Figure 3 can be used to determine this multiple and, thereby, the effect of finite size and load intensity on the stress distribution near the crack tip. Although cleavage is driven by stress and stressed volume, the difficulty of measuring critical values of these parameters dictates that fracture driving force, and thereby critical fracture conditions, be expressed in terms of more easily measured macroscopic parameters (e.g.  $J$  and  $CTOD$ ). Thus, an effective macroscopic driving force for cleavage fracture ( $J_{SSY}$ ) can be defined as follows:

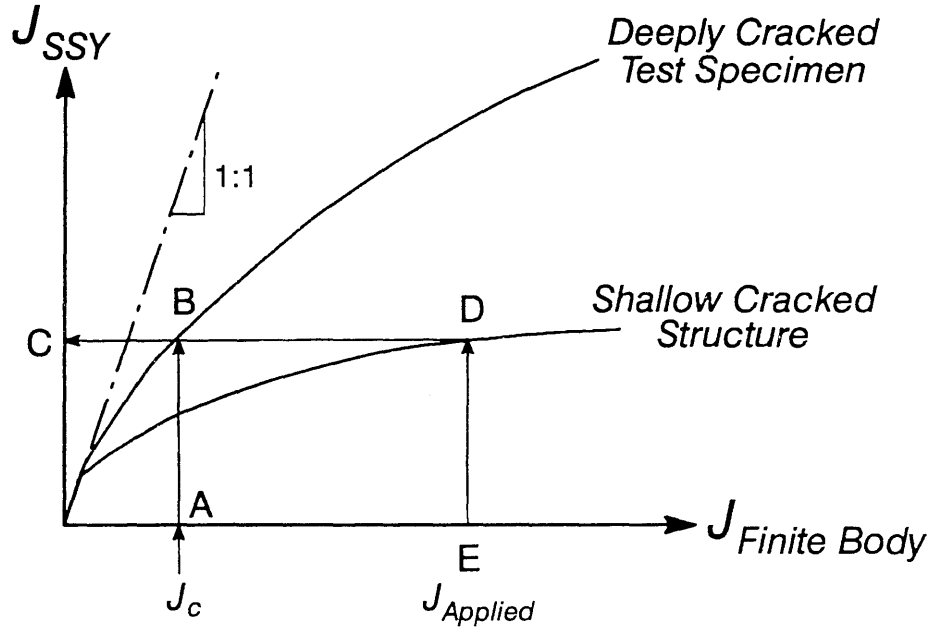


Figure 4: Conceptual variation of  $J_{SSY}$  with  $J$  for two finite bodies.

$J_{SSY}$  is the  $J$  to which the SSY model (infinite body) must be loaded to achieve the same stressed volume, and thereby the same likelihood of cleavage fracture, as in a finite body.

The variation of  $J_{SSY}$  with  $J$  is depicted schematically for two finite bodies in Figure 4. Upon initial loading of any finite body, crack-tip plasticity is well contained within a surrounding elastic field. Crack-tip conditions are well approximated by SSY and, up to some geometry dependent deformation level,  $J_{SSY} \approx J_{Finite Body}$ . Subsequent interaction of plasticity at the crack tip with plasticity resulting from overall deformation of the structure relaxes the kinematic constraint against plastic flow at the crack tip, thus reducing the stresses in the crack tip region below what they are in SSY at the same  $J$ . This reduces the micro-scale driving force for cleavage. Consequently, the finite body requires more applied- $J$  to achieve the same conditions for cleavage (same stressed volume) as in the infinite body. This finite size effect on crack-tip stress fields differs for different geometries constructed from the same material; it is indicated by deviation from the 1:1 slope in Figure 4. Information of this type is useful for both analysis of fracture test data and for assessing the defect integrity of structures. Path A-B-C on Figure 4 illustrates the procedure to remove geometric dependencies from experimental cleavage fracture toughness ( $J_c$ ) data by determining the geometry independent cleavage fracture toughness ( $J_{SSY}$ ) corresponding to a measured  $J_c$  value. Alternatively, Figure 4 permits determination of the effective driving force for cleavage fracture produced by structural loading to a certain  $J_{Applied}$  value (path E-D-C). Two different methods have been used to calculate  $J_{SSY}$  from finite element results, as discussed in the following sections.

### 2.3.1 Use of Crack Plane Stresses to Define $J_{SSY}$ [7]

The variation of the maximum principal stress on the crack plane with distance from the crack tip and deformation level is depicted in Figure 5 for the  $a/W=0.15$ ,  $n=10$  SE(B). These stresses have been

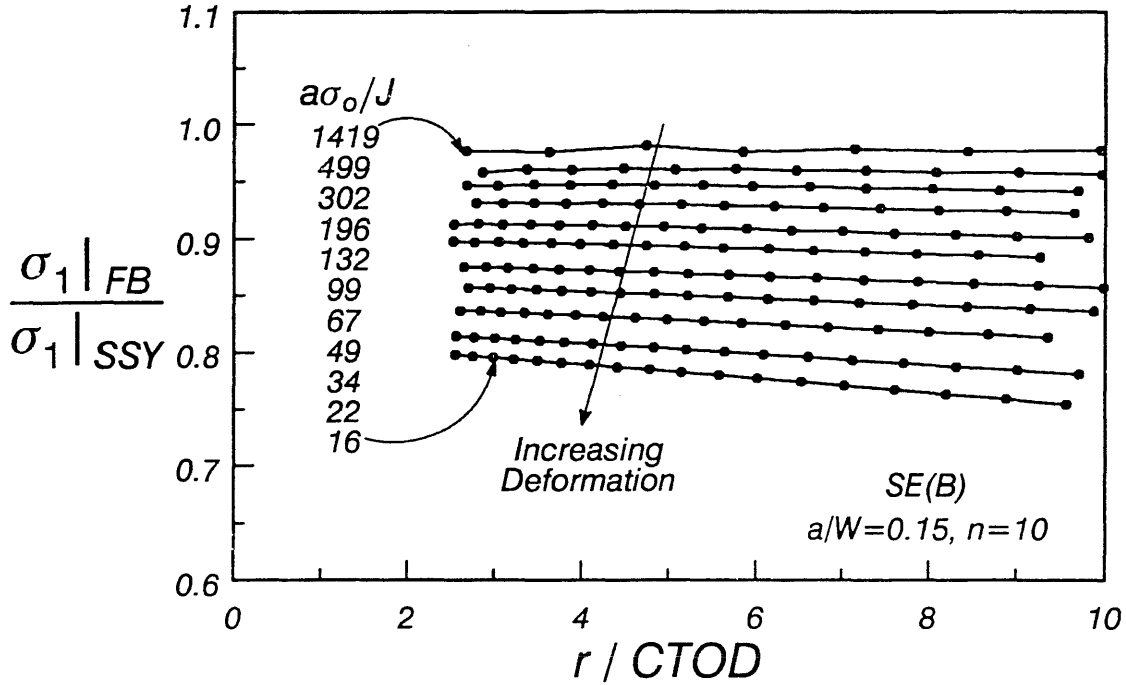


Figure 5: Variation of maximum principal stress on the crack plane with distance from the crack tip and applied  $-J$  for an  $a/W=0.15$   $n=10$  SE(B).

normalized by the stress that occurs in the SSY model at the same normalized distance ahead of the crack tip (same  $r/(J/(\alpha\sigma_o\epsilon_o))$ ) when loaded to the same  $J$  as the SE(B). The independence of these normalized stresses ( $\sigma_1|_{FB}/\sigma_1|_{SSY}$ ) with distance from the crack tip indicates the self similarity of the SSY and SE(B) stress distributions.  $J_{SSY}$  is calculated for each line on this graph as the  $J$  value required in the SSY model to achieve the same opening mode stress as in the finite body. The following equation is solved iteratively for  $J_{SSY}$  using a nonlinear root solver:

$$\frac{\sigma_1|_{FB}}{\sigma_o} = G_1 \left( \frac{r}{J_{SSY}/\alpha\sigma_o\epsilon_o} \right)^{G_2} \exp \left( G_3 \frac{J_{SSY}}{\alpha\sigma_o\epsilon_o} \right) \quad (2.3.1.1)$$

where

$\sigma_1|_{FB}$  finite body stress at  $r = 4\delta$

$\delta$  CTOD

$r$   $4\delta$

$G_i$  fit coefficients summarized in Table 1.

This functional form is adopted solely for convenience, i.e. a simple, closed form fit to the finite element SSY data.

The equivalence forced by eqn. 2.3.1.1 between SSY and finite body stresses at  $r = 4\delta$  corresponds to selecting the critical microstructural distance ( $l_o^*$ ) in the Richie–Knott–Rice model [10]. However, self-similarity between the SSY and finite body stress distributions makes the specific  $r/\delta$  value used unimportant over a wide range of deformation.  $J_{SSY}$  values are independent of the critical distance selected over a range of distances that encompasses fractographically determined  $l_o^*$  values [14–15],



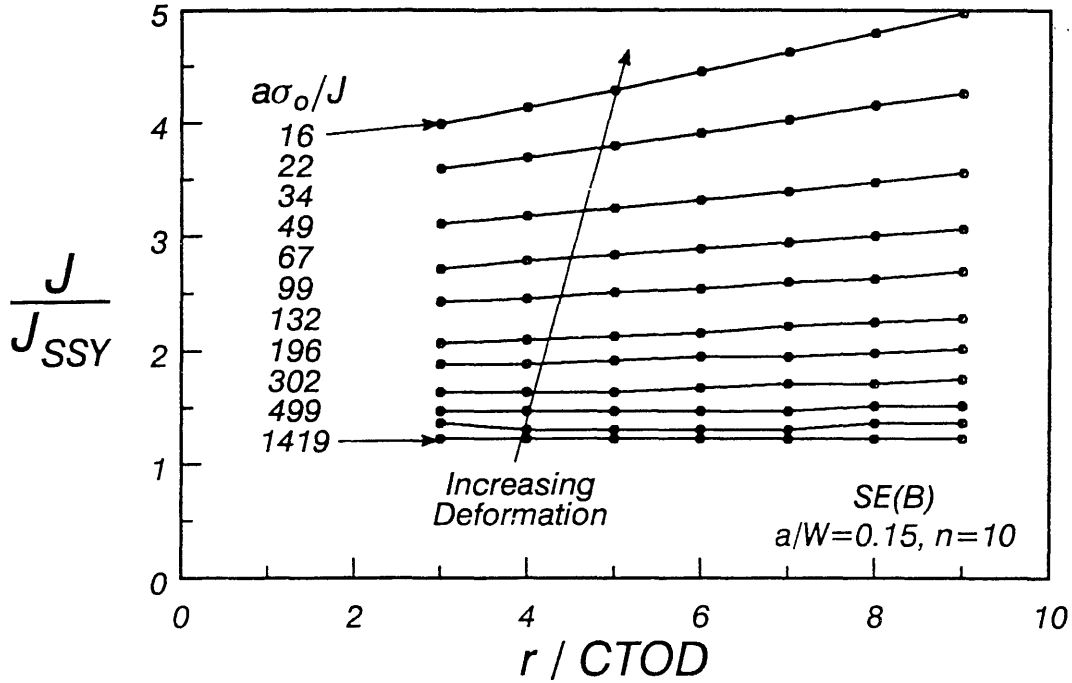


Figure 6: Dependence of  $J_{SSY}$  on critical distance ( $r/CTOD$ ) and applied  $-J$  for an  $a/W=0.15$   $n=10$  SE(B), as shown in Figure 6<sup>3</sup>. Predictions of the RKR model depend upon  $l_o^*$  because RKR uses the HRR fields as a reference solution. HRR is not self-similar to finite body stress distributions while  $SSY$  is. Thus, the ability to determine  $J_{SSY}$  irrespective of the actual  $l_o^*$  value relies on self-similar stress distributions around the crack in finite and infinite bodies.

Table 1: Fit coefficients for eqn. 2.3.1.1							
$n$	$G_1$	$G_2$	$G_3$	$n$	$G_1$	$G_2$	$G_3$
4.0	0.842	-0.2817	-0.926	10.0	1.801	-0.1169	-5.169
4.4	0.935	-0.2595	-1.403	12.8	1.989	-0.0926	-5.721
5.0	1.077	-0.2312	-2.181	18.0	2.219	-0.0668	-6.165
5.8	1.225	-0.2016	-3.057	26.5	2.413	-0.0467	-6.433
7.0	1.422	-0.1687	-3.952	50.0	2.646	-0.0255	-6.810
8.2	1.577	-0.1454	-4.446				
These coefficients can be linearly interpolated vs. $1/n$ , to estimate $SSY$ opening mode stresses on the crack plane within 0.75% for $2 \leq r/\delta \leq 10$ .							

### 2.3.2 Use of Stressed Areas to Define $J_{SSY}$ [9]

The variation of area enclosed by a principal stress contour ( $A_{FB}$ ) with contour level is depicted in Figure 7 for the  $a/W=0.15$ ,  $n=10$  SE(B). These areas are normalized by the area within this same contour in the  $SSY$  model ( $A_{SSY}$ ) when loaded to the same  $J$  as the SE(B). The area values for both the SE(B) and  $SSY$  solutions are determined by finite-element analysis. To simplify future applications

3. In practice,  $J_{SSY}$  is calculated by eqn 2.3.1.1 only if  $J_{SSY}$  values calculated at  $r=3\delta$  and at  $r=8\delta$  do not differ by more than  $\pm 10\%$  of their average value. A larger deviation would signal too great a dependence of  $J_{SSY}$  on the critical distance selected and, consequently, a breakdown of the method.

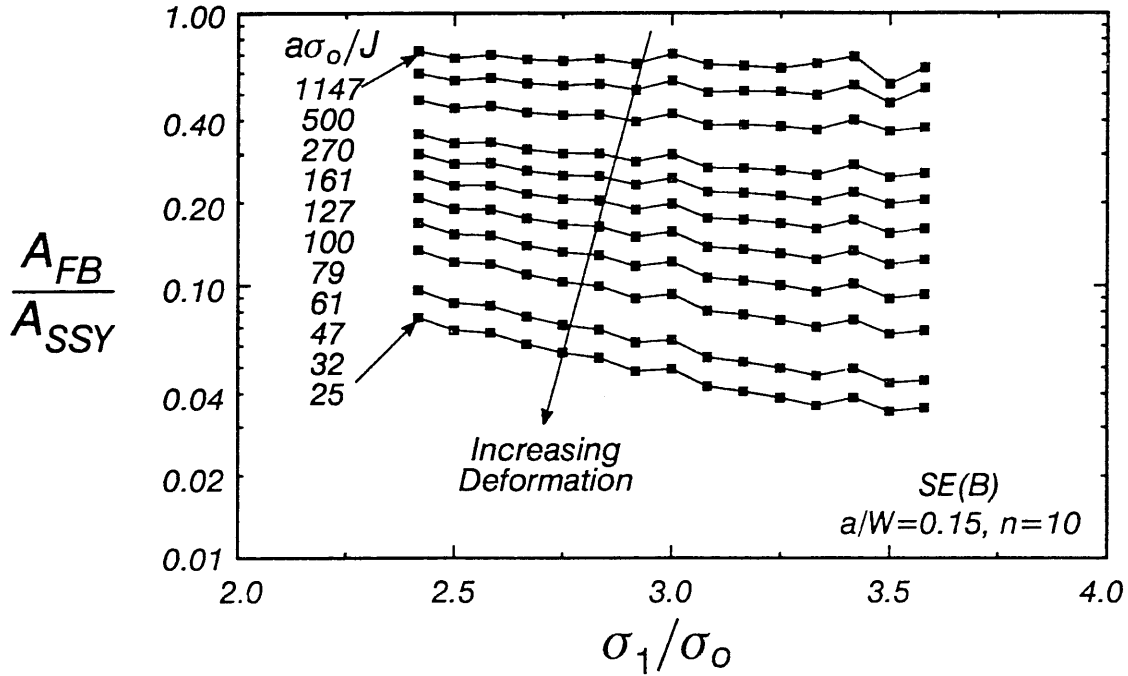


Figure 7: Variation of area within a principal stress contour with contour value and applied  $-J$  for an  $a/W=0.15$   $n=10$  SE(B).

of this technique, the  $SSY$  results are expressed as a closed-form function of principal stress ( $\sigma_1$ ) and strain hardening coefficient ( $n$ ):

$$\frac{A\sigma_o^2}{J_{SSY}^2} = 10^{f\left[\frac{\sigma_1}{\sigma_o}, n\right]} \quad (2.3.2.1)$$

$$f\left[\frac{\sigma_1}{\sigma_o}, n\right] = H_0 + H_1\left(\frac{\sigma_1}{\sigma_o}\right) + H_2\left(\frac{\sigma_1}{\sigma_o}\right)^2 + H_3\left(\frac{\sigma_1}{\sigma_o}\right)^3 + H_4\left(\frac{\sigma_1}{\sigma_o}\right)^4$$

where

$A$  area within a principal stress contour

$H_i$  fit coefficients summarized in Table 2

The independence of these normalized areas ( $A_{FB}/A_{SSY}$ ) with principal stress value indicates the self similarity of  $SSY$  and SE(B) stress distributions.  $J_{SSY}$  is calculated for each line on this graph as the  $J$  value required in the  $SSY$  model to achieve the same area within a principal stress contour as in the finite body. Solving eqn. 2.3.2.1 for  $J_{SSY}$  gives:

$$J_{SSY} = \sigma_o \sqrt{\frac{A_{FB}}{f\left[\frac{\sigma_1}{\sigma_o}, n\right]}} \quad (2.3.2.2)$$

where

$A_{FB}$  area within a contour  $\sigma_1 = 3\sigma_o$  in the finite body

This forced equivalence between  $SSY$  and finite body areas at  $\sigma_1 = 3\sigma_o$  corresponds to selecting the critical stress for cleavage fracture initiation ( $\sigma_f^*$ ) in the Richie Knott Rice model [10]. However, self-similarity between the  $SSY$  and finite body stress distributions makes the specific  $\sigma_1/\sigma_o$  value used

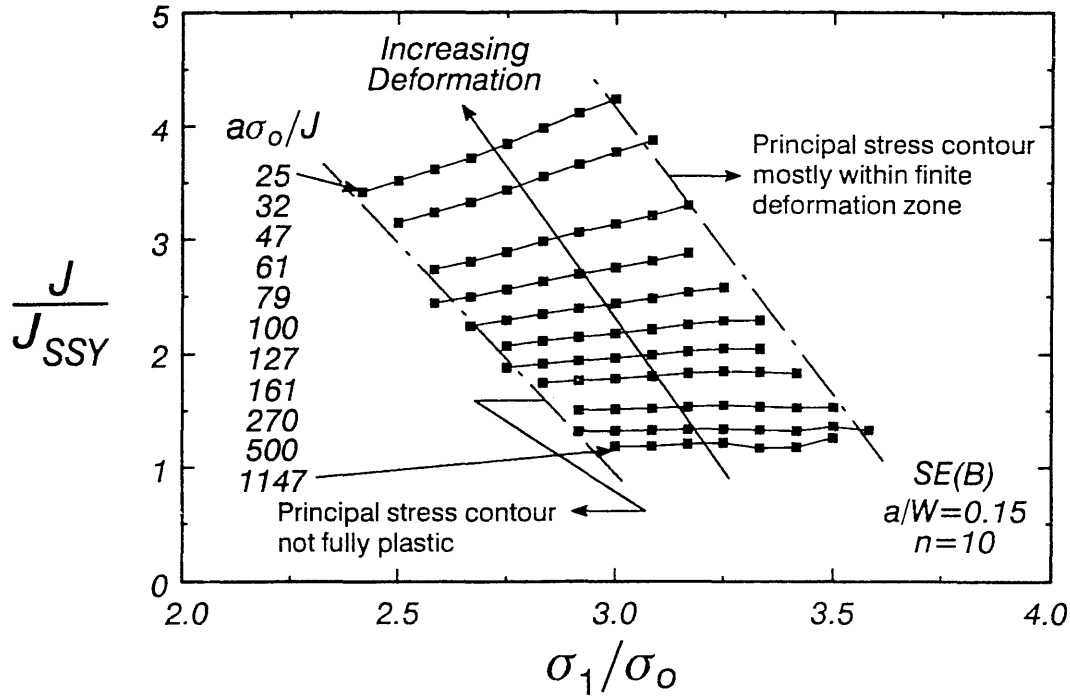


Figure 8: Dependence of  $J_{SSY}$  on critical stress ( $\sigma_1/\sigma_0$ ) and applied  $-J$  within the limits of principal stress contour validity for an  $a/W=0.15$   $n=10$  SE(B).

unimportant over a wide range of deformation.  $J_{SSY}$  values are independent of the cleavage fracture stress selected over a wide range, as shown in Figure 8<sup>4</sup>. Predictions of the RKR model depend upon  $\sigma_f^*$  because RKR uses the HRR fields as a reference solution. HRR is not self-similar to finite body stress distributions while SSY is. Thus, the ability to determine  $J_{SSY}$  irrespective of the actual  $\sigma_f^*$  value relies on self-similar stress distributions around the crack in finite and infinite bodies.

### 2.3.3 Comparison of these Techniques

Both the crack plane stress technique and the stressed volume technique for determining  $J_{SSY}$  require an assumption regarding a critical microstructural parameter that controls cleavage fracture initiation. Implementation of the crack plane stress technique requires assumption of the critical microstructural distance for cleavage fracture ( $l_o^*$ ) while the stressed volume technique requires assumption of the cleavage fracture stress ( $\sigma_f^*$ ). Fractographic and experimental studies show that both  $l_o^*$  and  $\sigma_f^*$  are material dependent. Further, their measurement is difficult and by no means standardized. However, self-similarity of the SSY and finite body stress distributions makes the actual  $l_o^*$  and  $\sigma_f^*$  values unimportant. Further, both the crack plane stress technique and the stressed volume technique produce very similar  $J_{SSY}$  values for SE(B) specimens, as shown in Figure 9. The crack plane stress technique is used in this study.

4. In practice,  $J_{SSY}$  is calculated by eqn 2.3.2.2 only if  $J_{SSY}$  values calculated at the limits of principal stress contour validity shown in Figure 8 do not differ by more than  $\pm 10\%$  of their average value. A larger deviation would signal too great a dependence of  $J_{SSY}$  on the critical stress selected and, consequently, a breakdown of the method.

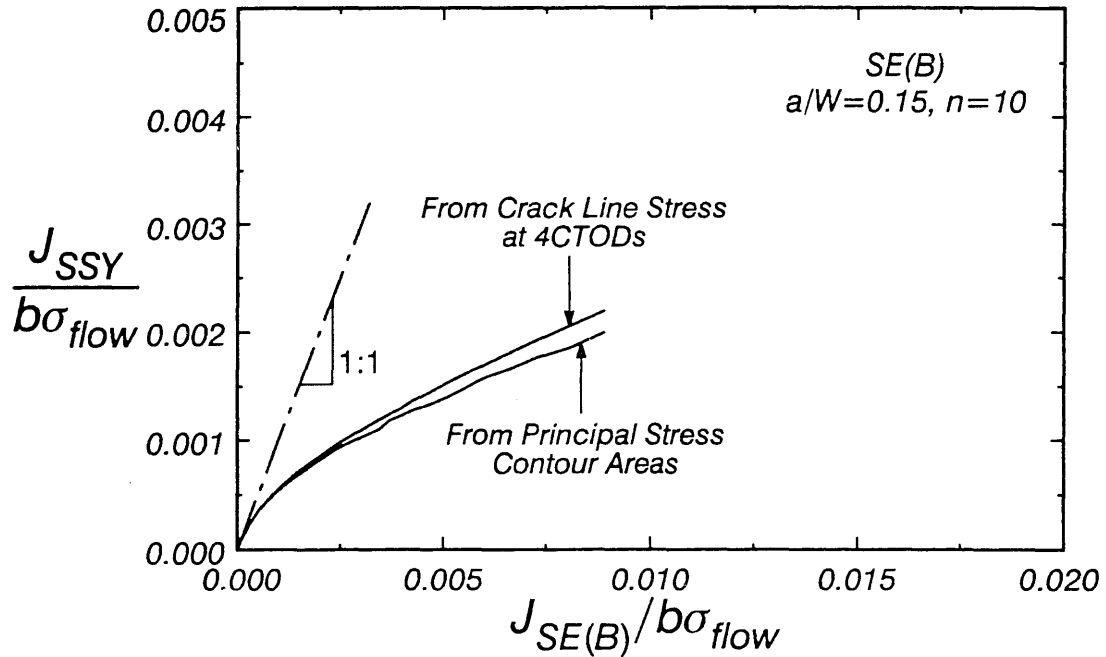


Figure 9: Comparison of  $J_{SSY}$  values determined using the crack plane stress and stressed area techniques for an  $a/W=0.15$   $n=10$  SE(B).

Table 2: Fit coefficients for eqn. 2.3.2.1

$n$	$H_0$	$H_1$	$H_2$	$H_3$	$H_4$	Minimum $\sigma_1/\sigma_o$	Maximum $\sigma_1/\sigma_o$
4.0	6.4306	-2.4711	0.5037	-0.07975	0.00552	2.0	4.0
5.0	6.2579	-2.1653	0.3749	-0.06603	0.00505	2.0	4.0
7.0	6.3835	-2.3504	0.5679	-0.14132	0.01224	2.0	3.9
8.5	6.6570	-2.7970	0.8741	-0.22819	0.01917	2.0	3.7
10.0	7.6641	-4.3138	1.7368	-0.43685	0.03560	2.0	3.6
12.5	7.8091	-4.3940	1.6983	-0.38870	0.02350	2.0	3.4
15.0	3.3057	3.0253	-2.8580	0.86107	-0.10728	2.0	3.4
17.5	1.6667	6.0670	-4.9547	1.50771	-0.18342	2.0	3.3
20.0	-3.2613	14.4338	-10.2659	3.01033	-0.34420	2.0	3.2
23.5	-12.5856	30.1836	-20.2091	5.80089	-0.63903	2.0	3.2
27.0	-20.4631	43.6584	-28.8290	8.25238	-0.90134	2.0	3.1
32.0	-33.6117	65.9611	-42.9729	12.23590	-1.32269	2.0	3.1
35.0	-32.1490	63.8374	-41.8794	12.01090	-1.30924	2.0	3.0
39.0	-40.4790	78.0250	-50.9189	14.56910	-1.58107	2.0	3.0
42.0	-33.4180	66.2799	-43.6497	12.58860	-1.38113	2.0	2.9
50.0	-41.7313	80.6029	-52.8913	15.24150	-1.66755	2.0	2.9

Normalized areas within a principal stress contour in SSY at any  $n$  can be found to within 1.5% by linearly interpolating the normalized areas for two  $n$  values in this table bounding the  $n$  of interest.

### 3. APPROACH

Currently,  $J_{SSY}$  for welded SE(B) specimens can be estimated from published results for homogeneous specimens [6–7]. However, mismatch between weld metal and baseplate strength alters the deformation patterns in such specimens, causing potential errors in  $J_{SSY}$  determined by assuming specimen homogeneity. In this study, plane–strain elastic–plastic finite element analyses of SE(B) specimens containing a variety of common weld groove details are performed. The crack–tip stress fields quantified by these analyses permit evaluation of the variation of  $J_{SSY}$  with  $J$  for welded SE(B) specimens. This information establishes a baseline to judge the applicability of estimating  $J_{SSY}$  for a welded specimen from an analysis that takes no account of weld mismatch. The cases illustrated in Figure 10 are each modelled as 20% overmatched, homogeneous (no weld), and 20% undermatched. Unless indicated otherwise, the constitutive properties detailed in Table 3 are used. The weldment is modelled as a bi–material with no transition zone (heat affected zone, or HAZ) placed between the weld and the plate. The strain hardening exponents in Table 3 are calculated from yield stress based on an experimental correlation applicable to construction steels developed by Barsom and Rolfe[16]:

$$n = \left[ \frac{\sigma_o}{15} \right]^{\frac{4}{3}} \quad (\sigma_o \text{ is in ksi}) \quad (3.1)$$

Certain aspects of this approach, adopted for expediency, require justification to ensure the applicability of these results to real weldments. For example, modelling a weldment as a bi–material calls into question the applicability of these results to weldments having a constitutive property gradient across the HAZ. Further issues include

1. The calculation of strain hardening capacity from yield strength using eqn. (3.1), while physically realistic, provides different absolute hardening capacities dependent upon the plate yield strength selected for analysis. It is not apparent, for example, that the results of an analysis of a 20% undermatched weld joining 60 ksi yield strength steel (plate  $n = 6.3$ , weld  $n = 4.7$ ) apply to a 20% undermatched weld joining 100 ksi yield strength steel (plate  $n = 12.5$ , weld  $n = 9.3$ ).

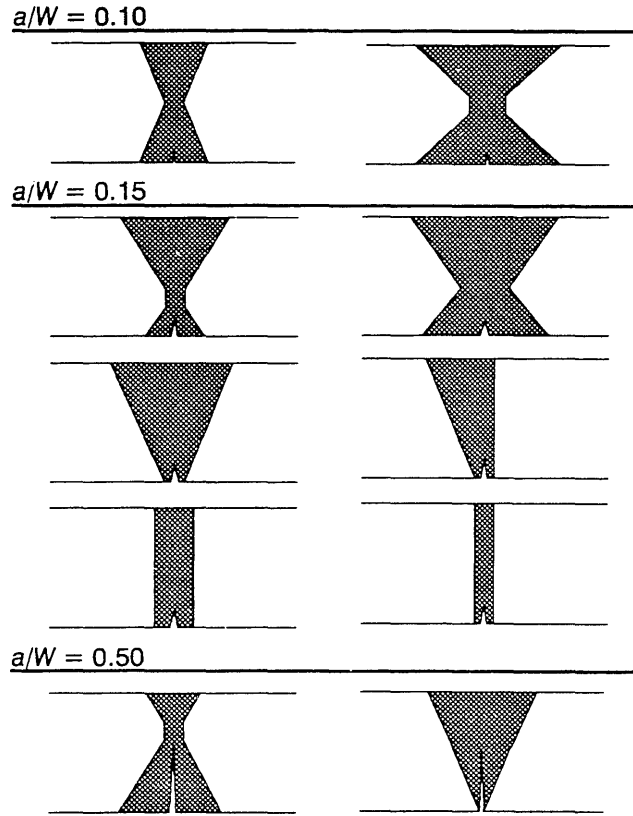


Figure 10: Weldment geometries analyzed.

2. Quite large amounts of overmatch can occur in practice (e.g. welding A36 steel with an E7018 electrode producing approximately 50% overmatch) which lie outside the primary focus of this study.

This investigation addresses each of these issues.

Table 3: Constitutive properties for weldment analyses				
% Mismatch	Weld		Plate	
	$\sigma_o$ [ksi]	$n$	$\sigma_o$ [ksi]	$n$
20% Over	104	13	86	10
No Weld	---	--	104	13
20% Under	104	13	130	18
<p>Yield strength (<math>\sigma_o</math>) and strain hardening exponent (<math>n</math>) are coefficients in the Ramberg–Osgood constitutive relation:</p> $\frac{\epsilon}{\epsilon_o} = \frac{\sigma}{\sigma_o} + \alpha \left( \frac{\sigma}{\sigma_o} \right)^n$ <p>where <math>\alpha = 1</math> and <math>\epsilon_o = E/\sigma_o</math></p>				

## 4. FINITE ELEMENT MODELLING

Two-dimensional, plane-strain finite element analyses of SE(B) specimens are performed using conventional small strain theory. These analyses are conducted using the POLO–FINITE analysis software [17] on an engineering workstation.

Uniaxial stress–strain behavior is described using the Ramberg–Osgood model

$$\frac{\epsilon}{\epsilon_o} = \frac{\sigma}{\sigma_o} + \alpha \left( \frac{\sigma}{\sigma_o} \right)^n \quad (4.1)$$

where  $\sigma_o$  is the reference stress (0.2% offset yield),  $\epsilon_o = \sigma_o/E$  is the reference strain,  $\alpha$  is a dimensionless parameter, and  $n$  is the strain hardening coefficient.

$J_2$  deformation plasticity theory (i.e. nonlinear elasticity) describes the multi-axial material behavior. Total strains and total stresses are related by

$$\epsilon_{ij} = \left[ \frac{1+\nu}{E} + \frac{3\alpha\epsilon_o}{2\sigma_o} \left( \frac{\sigma_e}{\sigma_o} \right)^{n-1} \right] s_{ij} + \frac{1-2\nu}{3E} \sigma_{kk} \delta_{ij} \quad \sigma_e = \sqrt{\frac{3}{2} s_{ij} s_{ij}} \quad (4.2)$$

where  $s_{ij}$  is the stress deviator,  $\sigma_e$  is the Mises equivalent tensile stress,  $\sigma_{kk}$  is the trace of the stress tensor, and  $\delta_{ij}$  is the Kronecker delta.

Analysis of the SSY model is identical to that described previously by Dodds, et al. [7]. Finite element models are constructed for each combination of  $a/W$  ratio and weld joint geometry. These computations apply to SE(B) specimens of standard proportions; the unsupported span is four times the specimen width. Models of symmetric joints contain approximately 900 elements and 2850 nodes, while the non-symmetric mesh of the single bevel weld contains 1414 elements and 4431 nodes. Fig-

ure 11 illustrates this model. Eight noded, plane-strain isoparametric quadrilateral elements are used throughout. Reduced (2 x 2) Gaussian integration is used to eliminate locking of the elements under incompressible plastic deformation. A semi-circular core of elements surrounds the crack tip in all models. This core consists of eight equally sized wedges,  $22.5^\circ$  each, of elements in the  $\theta$  direction. Each wedge contains 30 quadrilateral elements whose radial dimension decreases geometrically with decreasing distance to the crack tip. The eight crack-tip elements are collapsed into wedges with the initially coincident nodes left unconstrained to permit development of crack-tip blunting deformations. The side nodes of these elements are retained at the mid-point position. This modelling technique produces a  $1/r$  strain singularity<sup>5</sup>, appropriate in the limit of perfect plasticity. Crack-tip element size ranges from 0.2% to 0.02% of the crack depth depending on the crack depth modelled.

Load is distributed uniformly over two small elements at the center of the compression face of the specimen to eliminate the local singularity effects caused by a concentrated nodal load. Between 30 and 50 variably sized load steps are taken to deform the specimen until the  $CTOD \geq 0.05a$ . Strict criteria at each step ensure convergence of calculated stresses and strains to the third significant figure. Two to three full Newton iterations at each load step are generally required to satisfy this criteria. As deformation plasticity is strain path independent, converged solutions are load step size invariant.

The  $J$ -integral is computed at each load step using a domain integral method [18–19].  $J$  values calculated over domains adjacent to and remote from the crack tip, but not crossing a bi-material interface, are within 0.003% of each other, as expected for deformation plasticity combined with these detailed meshes. All  $J$  values reported for weldments are calculated over domains that lie completely within the weld metal [20].  $CTOD$  is estimated from the blunted shape of the crack flanks using the Rice  $45^\circ$  intercept procedure. LLD is taken as the relative displacement in the loading direction of a node on the symmetry plane located approximately  $0.4b$  in front of the crack tip and of a node located

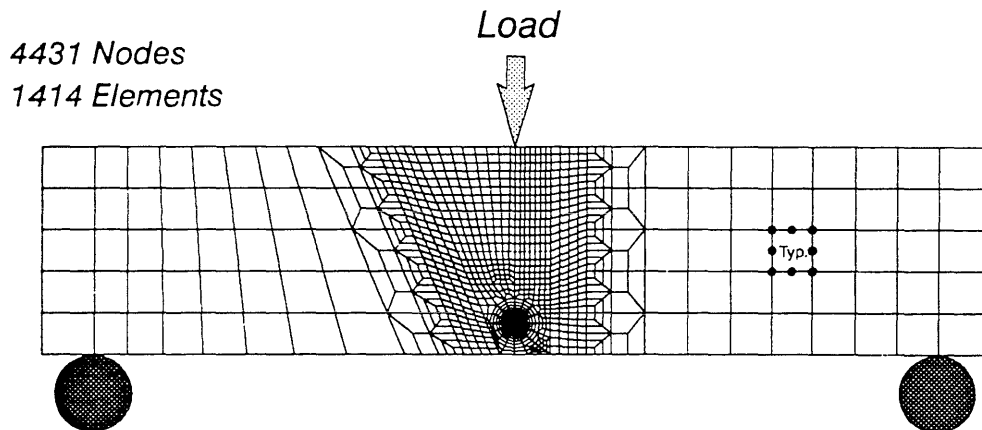


Figure 11: Finite element model of a SE(B) specimen containing an  $a/W = 0.15$  crack in a single bevel joint.

5.  $r$  is distance from the crack tip.

a distance  $W/2$  above the support. This procedure eliminates the effect of locally high displacements in the vicinity of both the load and support points on the LLD.

## 5. RESULTS AND DISCUSSION

### 5.1 Finite Element Results for $\pm 20\%$ Mismatch

The constraint correction curve illustrated schematically in Figure 4 is shown quantitatively in Figure 12 for two welds containing  $a/W=0.15$  cracks:  $60^\circ$  Double-V with a 0.2-inch root gap and  $70^\circ$  Double-V with a 0.5-inch root gap.  $J_{SSY}$  for some welds (e.g.  $70^\circ$  Double-V) is independent of  $\pm 20\%$  mismatch, indicating that while mismatch alters plasticity distribution throughout the specimen, the near-tip stresses are unaffected. Other welds, e.g.  $60^\circ$  Double-V, have some effect on  $J_{SSY}$ . However, the virtually limitless number of weld joint geometry / crack depth combinations preclude calculation of  $J_{SSY}$  for each individual case. In view of the small effect of  $\pm 20\%$  mismatch on  $J_{SSY}$ , even for the  $60^\circ$  Double-V weld, the following therefore seems a useful and reasonable approximation:

$$J_{SSY}|_{WELD} = J_{SSY}|_{\substack{HOMOGENEOUS \\ (ALL\ WELD\ METAL)}} \quad (5.1.1)$$

This ‘all weld metal’ approximation, if sufficiently accurate, enables  $J_{SSY}$  estimation from previously published solutions for homogeneous SE(B)s [6–7]. As finite element models which fully resolve near-tip fields and account for the weld / plate interface are quite detailed, considerable effort can be saved if the all weld metal approximation is sufficiently accurate.

The following error measure is defined to evaluate the accuracy of the all weld metal approximation:

$$Error = \frac{J_{SSY}|_{WELD} - J_{SSY}|_{\substack{HOMOGENEOUS \\ (ALL\ WELD\ METAL)}}}{J_{SSY}|_{WELD}} \cdot 100 \quad (5.1.2)$$

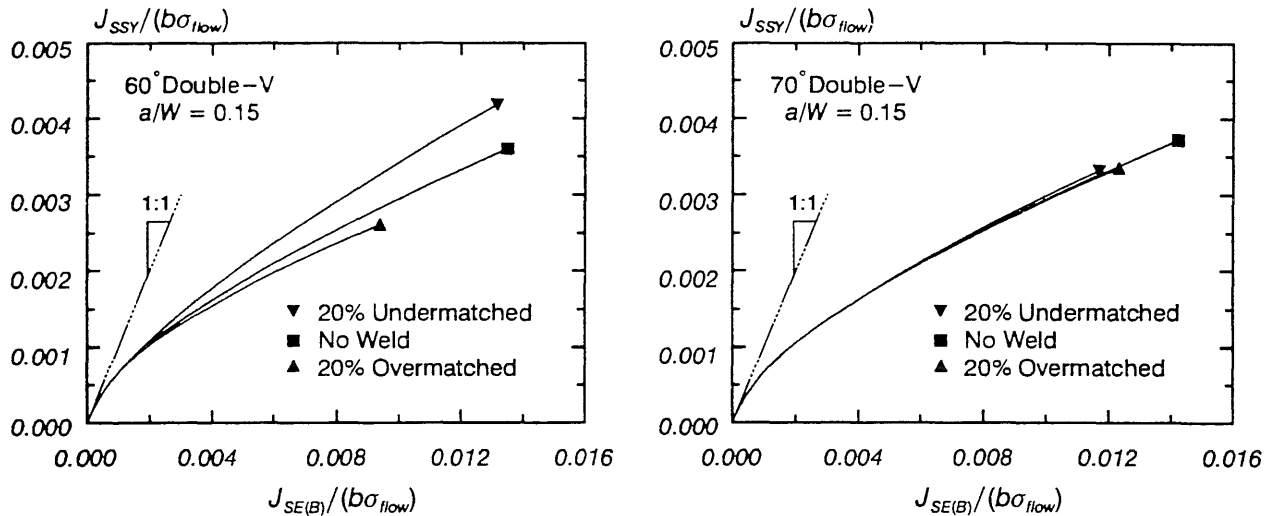


Figure 12: Constraint correction curves for two  $\pm 20\%$  mismatched welds containing  $a/W=0.15$  cracks.



The variation of  $J_{SSY}$  estimation error with normalized  $J_{SE(B)}$  is illustrated in Figure 13 for all of the welds analyzed. Even though all of the errors are reasonably small, certain weld joint / crack depth combinations have much greater effects than others. While a considerable number of cases have been analyzed, situations producing a greater effect on  $J_{SSY}$  may remain undiscovered. It therefore seems useful to determine what factors promote deviation of  $J_{SSY}$  from the homogeneous solution. Certainly the minimum distance from the crack tip to the weld/plate interface ( $L_{min}$ ) should play an important role. If  $L_{min}$  is large, it seems unlikely that weld mismatch could significantly alter the crack tip stress fields used to calculate  $J_{SSY}$ . Conversely, narrow weld joints ( $L_{min}$  small) may have some influence, particularly as  $L_{min}$  approaches the length scale over which  $J_{SSY}$  is calculated. The variation of  $J_{SSY}$  estimation error with  $L_{min}$  at two fixed applied- $J$  levels is shown in Figure 14 for all weldments analyzed. These data demonstrate that, even at very high applied- $J$ , there is virtually no effect of  $\pm 20\%$  mismatch on  $J_{SSY}$  if  $L_{min}$  exceeds 0.2-inches. For welds having  $L_{min}$  smaller than 0.2-inches, reasonably accurate  $J_{SSY}$  estimation is possible by eqn. 5.1.1 until the applied deformation becomes so large that significant interaction occurs between the stress field at the weld / plate interface and the stress field at the crack tip. The information in Figure 14 can be used to determine the relationship between  $L_{min}$  and the deformation level above which accurate  $J_{SSY}$

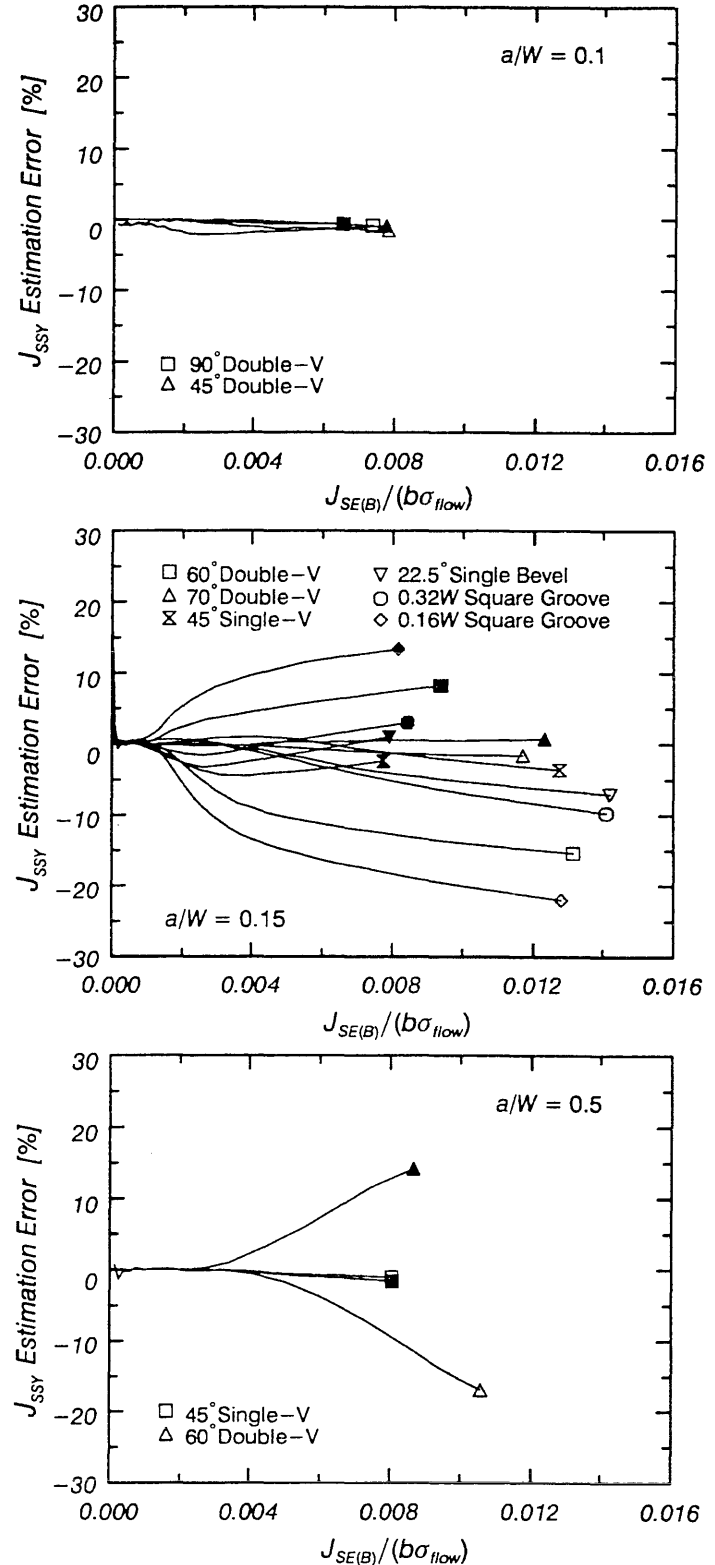


Figure 13: Variation of  $J_{SSY}$  estimation error with applied- $J$  for  $\pm 20\%$  mismatched welds. Filled symbols represent overmatching, open symbols undermatching.

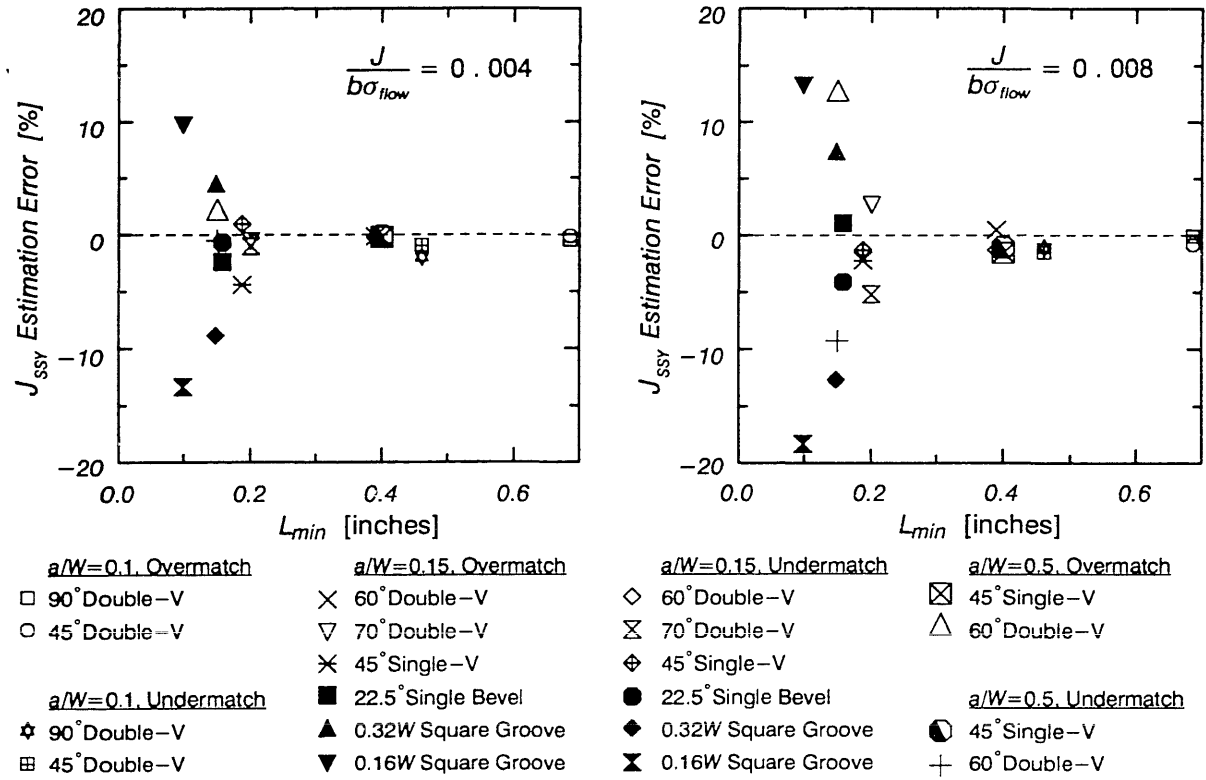


Figure 14: Variation of  $J_{SSY}$  estimation error at two fixed applied- $J$  levels with minimum distance from the crack tip to the weld/plate interface for  $\pm 20\%$  mismatched welds.

estimation by eqn. 5.1.1 is no longer possible, as illustrated in Figure 15. The variation of weld size to produce less than 10%  $J_{SSY}$  estimation error with applied- $J$  for  $\pm 20\%$  mismatched weldments is given in Figure 16. This curve can be used as a basis to judge whether accurate determination of  $J_{SSY}$  requires finite element analysis of the actual weldment ( $J_c - L_{min}$  combinations above the curve) or if published solutions for homogeneous SE(B)s provide sufficient accuracy ( $J_c - L_{min}$  combinations below the curve).

## 5.2 Justification of Assumptions in Approach

### 5.2.1 HAZ Modelling

The results presented in the preceding section are determined using finite element models which do not account for the transition in constitutive properties between the weld and the plate. The HAZ is so remote from a crack on the weld centerline and is so thin that it should have little effect on the stresses near the crack tip used to calculate  $J_{SSY}$ . To demon-

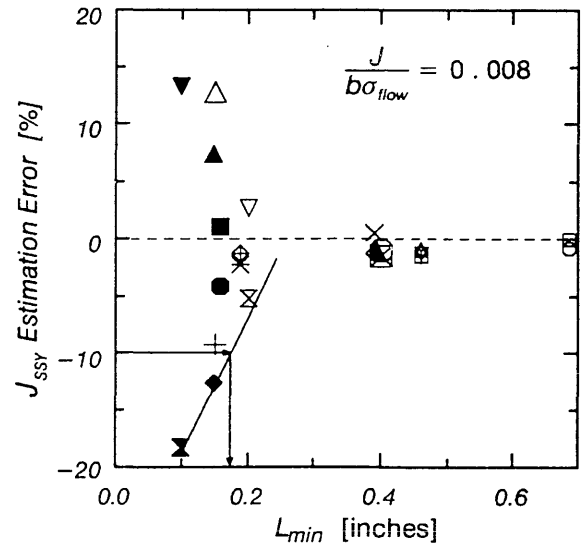


Figure 15: Determination of distance needed from the crack tip to the weld/plate interface to keep  $J_{SSY}$  estimation error below 10% for  $\pm 20\%$  mismatched welds.

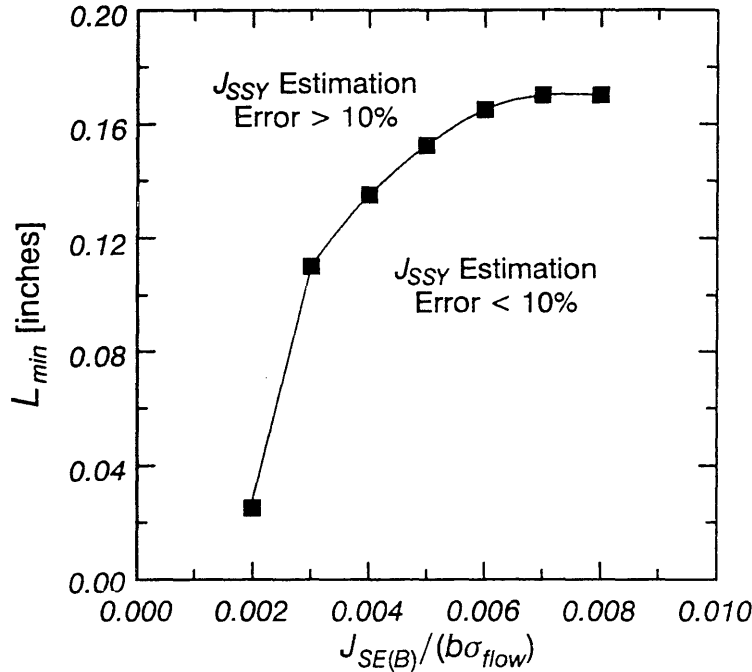


Figure 16: Effect of applied  $-J$  on distance needed from the crack-tip to the weld/plate interface to keep  $J_{SSY}$  estimation error below 10% for  $\pm 20\%$  mismatched welds.

strate the validity of ignoring the HAZ, analyses of the two shallow cracked square groove weldments including a highly refined HAZ are performed. Groove widths are  $0.16W$  and  $0.32W$ , producing  $L_{min}$  values of 0.1-inches and 0.2-inches, respectively. A detail of the  $0.16W$  square groove model near the crack is shown along with the constitutive properties used to model the HAZ in Figure 17. The yield strength of the 0.005-inch wide HAZ layer immediately adjacent to the weld is 180 ksi, characteristic of the as-quenched martensite found in the grain coarsened HAZ. Between this high hardness layer and the plate, the HAZ is modelled as seven discrete layers of increasing width and decreasing strength. These models realistically represent both peak hardness and total HAZ width. Further, this model presents a greater challenge for accurate  $J_{SSY}$  estimation than occurs

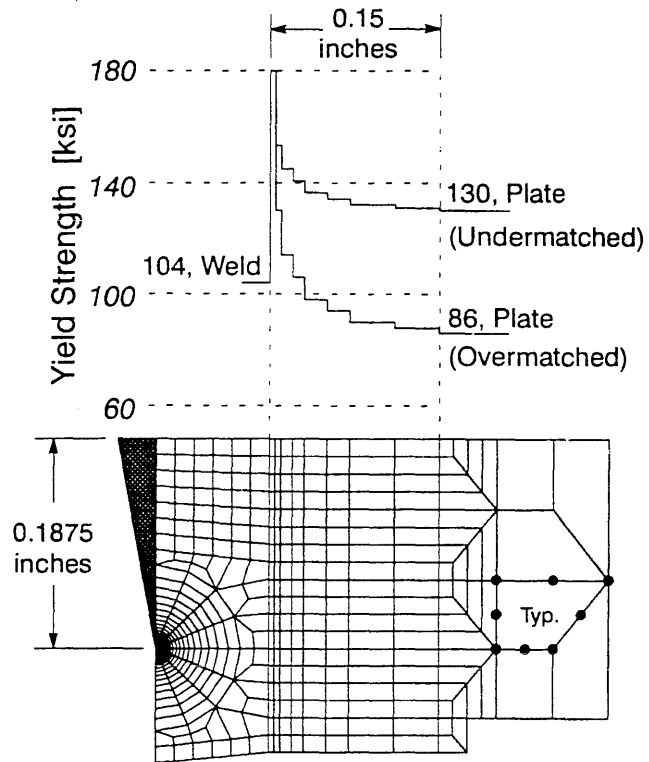


Figure 17: Finite element mesh detail and yield properties for  $0.16W$  square groove HAZ model.  $n$  is calculated from yield strength by eqn. 3.1.

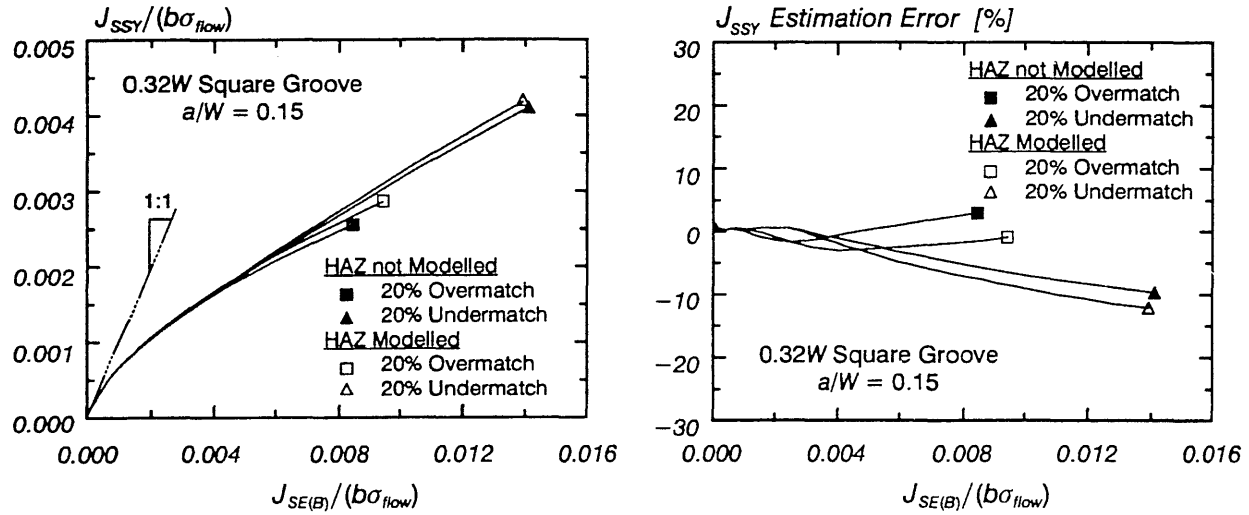


Figure 18: Effect of HAZ modelling on constraint correction curve for the 0.32W square groove weld.

in an actual weldment. An actual multi-pass weldment has a discontinuous high strength layer due to re-tempering from multiple passes, rather than the continuous high strength layer modelled here. The effect of HAZ modelling on the constraint correction curve for the 0.32W square groove weld is illustrated in Figure 18. Here the HAZ has negligible effect on  $J_{SSY}$  because the weld / plate interface is sufficiently remote from the crack tip ( $L_{min} \geq 0.2$ -inches). This is consistent with previous observations based on welds with no transition zone between the plate and the weld. However, as the distance between the crack tip and the weld / plate interface reduces, the presence of a high hardness HAZ significantly affects  $J_{SSY}$ , as shown in Figure 19 for the 0.16W square groove weldment. The expectation from analyses where the HAZ is ignored (Figure 16) is that a weldment with  $L_{min} = 0.1$ -inches will have  $J_{SSY}$  estimation errors below 10% if  $J_{SE(B)} / (b\sigma_{flow}) \leq 0.0028$ . This prediction is slightly non-conservative, for the 20% undermatched 0.16W square groove modelled with a HAZ, which has a  $J_{SSY}$  estimation error of 13% at  $J_{SE(B)} / (b\sigma_{flow}) = 0.0028$ . However, as noted previously, the high strength

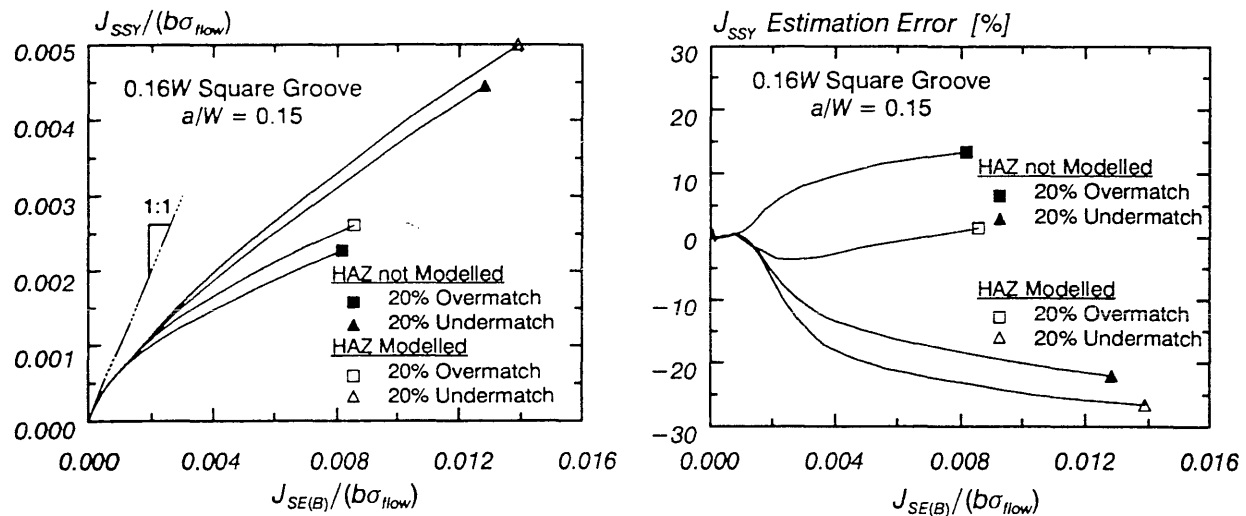


Figure 19: Effect of HAZ modelling on constraint correction curve for the 0.16W square groove weld.

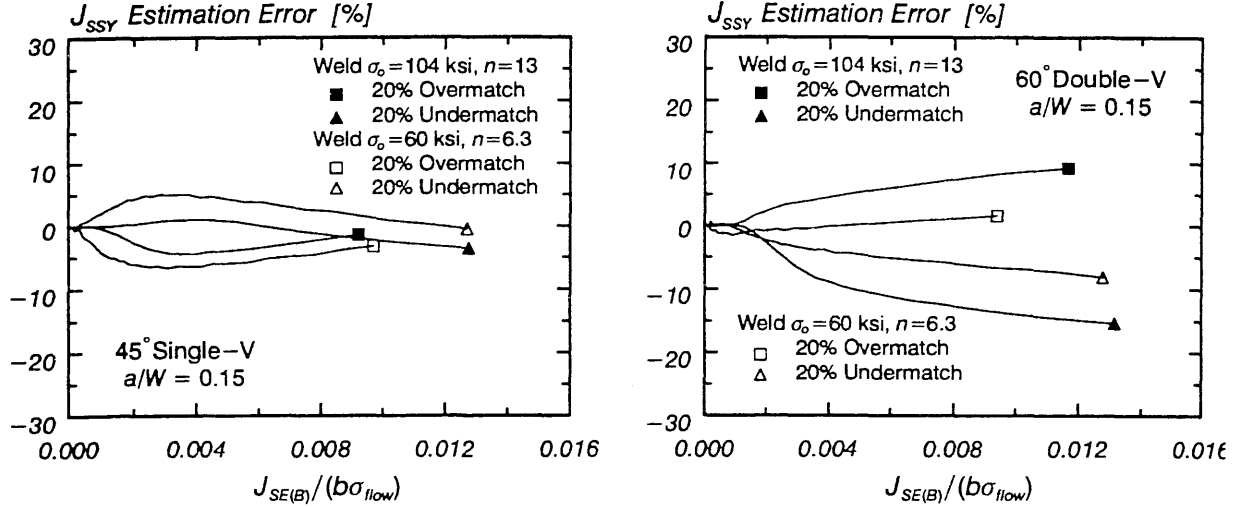


Figure 20: Effect of constitutive properties on  $J_{SSY}$  estimation accuracy for two welds containing  $a/W=0.15$  cracks.

HAZ is discontinuous in an actual multi-pass weldment, rather than continuous as modelled here. Thus, it does not appear that expectations regarding  $J_{SSY}$  estimation accuracy based on the simpler bi-material models are grossly inaccurate for real weldments with a constitutive property gradient across the HAZ.

### 5.2.2 Effect of Constitutive Properties

All of the results discussed thus far are generated using the constitutive properties detailed in Table 3. To assess the applicability of these results to mismatch for different constitutive properties, two weldments (45° Single-V and 60° Double-V) containing  $a/W=0.15$  cracks are analyzed using properties characteristic of a lower strength steel, given in Table 4. These two weldments are selected as they have  $L_{min}$  values that are near ( $L_{min} = 0.19$ –inches for 45° Single-V) and below ( $L_{min} = 0.15$ –inches for 60° Double-V) the 0.2–inch cutoff above which negligible effects of  $\pm 20\%$  mismatch on  $J_{SSY}$  are observed (Section 5.1).  $J_{SSY}$  estimation errors remain within previously established error bounds for both weldments considered, as illustrated in Figure 20. Thus, the effect of  $\pm 20\%$  mismatch on  $J_{SSY}$  estimation accuracy discussed in Section 5.1 appears approximately correct irrespective of the baseline  $\sigma_o$  and  $n$  values used in the finite element analysis.

Table 4: Constitutive properties for weldment analyses				
% Mismatch	Weld		Plate	
	$\sigma_o$ [ksi]	$n^1$	$\sigma_o$ [ksi]	$n^1$
20% Over	60	6.3	50	5.0
No Weld	---	---	60	6.3
20% Under	60	6.3	75	8.5
1. $n$ calculated from yield strength by eqn. (3.1)				

### 5.2.3 Effect of Extreme Overmatch

All results previously presented are for  $\pm 20\%$  mismatch. However, certain construction practices cause considerably greater overmatch. This is investigated by performing supplemental analysis for three  $a/W=0.15$  weldments:  $70^\circ$  Double-V,  $45^\circ$  Single-V, and  $60^\circ$  Double-V having  $L_{min}$  values of 0.39, 0.19, and 0.15-inches, respectively. The  $J_{SSY}$  estimation errors caused by mismatch ranging from 20% under to 100% over are given in Figure 21. The final point on these graphs indicates the last load step at which the stress field near the crack tip in the SE(B) is sufficiently self-similar to the SSY reference solution that  $J_{SSY}$  remains independent of the critical distance selected for its calculation. The data in Figure 21 indicate that both increased overmatching and small  $L_{min}$  values limit the maximum applied  $-J$  for SE(B) – SSY self-similarity. Over the range of applied  $-J$  that  $J_{SSY}$  can be calculated, the  $J_{SSY}$  estimation error for the two Double-V welds associated with 50% and 100% overmatch is approximately the same as for  $\pm 20\%$  mismatch. However,  $J_{SSY}$  estimation error for the Single-V weld is increased significantly by extreme overmatching.  $L_{min}$  parameterizes the departure of  $J_{SSY}$  for a weld from that for a homogeneous SE(B) at  $\pm 20\%$  mismatch irrespective of joint geometry. This simplification breaks down for greater levels of overmatching where weld geometry becomes important.

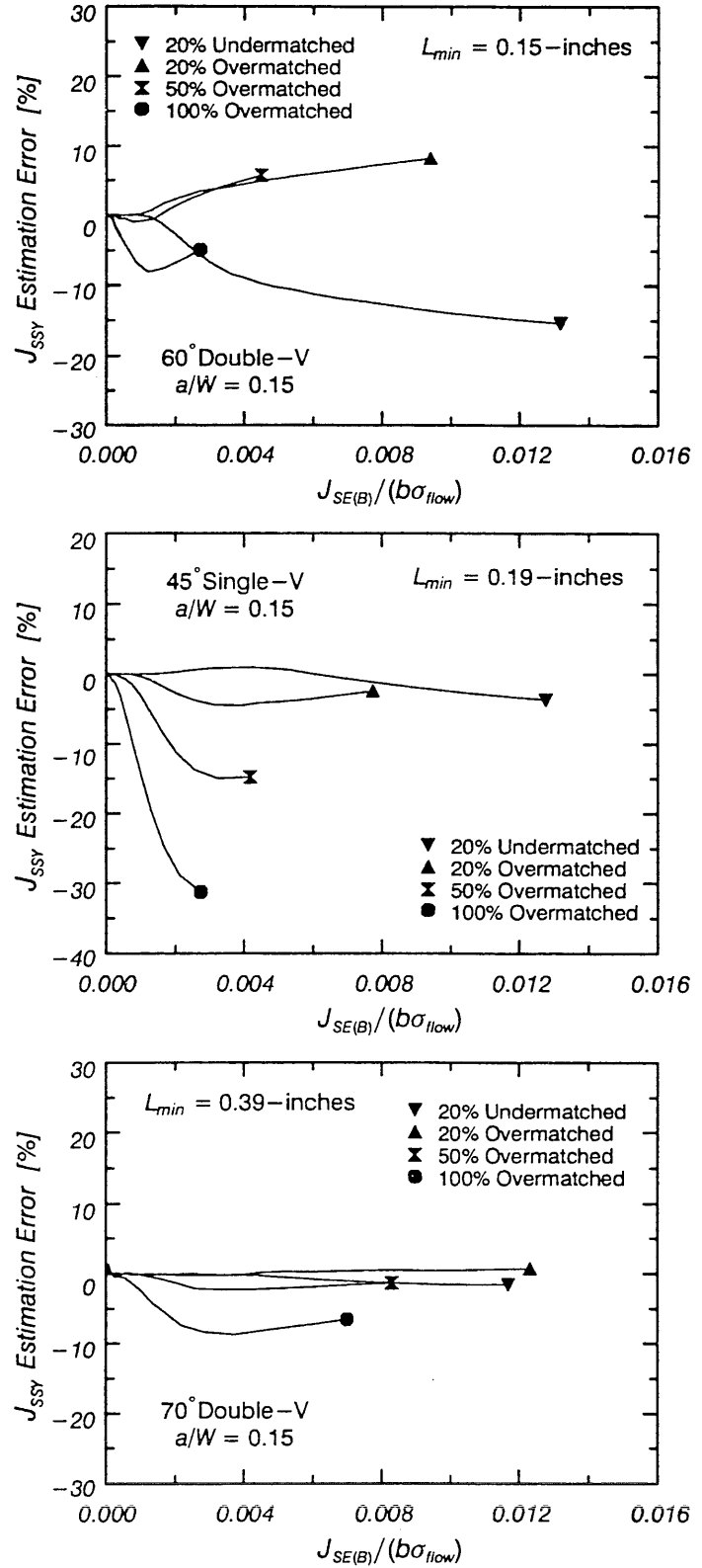


Figure 21: Effect of extreme overmatch on  $J_{SSY}$  estimation error for three welds containing  $a/W=0.15$  cracks.

## 6. SUMMARY AND CONCLUSIONS

Dodds and Anderson provide a framework to quantify finite size effects on cleavage fracture toughness when failure occurs at deformation levels where  $J$  no longer uniquely describes the state of stresses and strains in the vicinity of the crack tip. Size effects on cleavage fracture are quantified by defining a value termed  $J_{SSY}$ : the  $J$  to which an infinite body must be loaded to achieve the same stressed volume, and thereby the same likelihood of cleavage fracture, as in a finite body. In weld metal fracture toughness testing, mismatch between weld metal and baseplate strength can alter deformation patterns, which complicates size effects on cleavage fracture toughness. However, the virtually limitless number of weld joint geometry / crack depth combinations preclude calculation of  $J_{SSY}$  for each individual case. This study addresses the accuracy with which  $J_{SSY}$  for a welded single edge notch bend, SE(B), specimen can be approximated by previously published results for homogeneous specimens. The case of a crack located on the weld joint centerline is treated. The combined effects of weld groove type, degree of mismatch, and crack depth to specimen width ( $a/W$ ) ratio are considered by performing plane-strain elastic-plastic finite element analyses of SE(B) specimens containing a variety of common weld groove details. These results demonstrate virtually no effect of  $\pm 20\%$  mismatch on  $J_{SSY}$  if the distance from the crack tip to the weld/plate interface ( $L_{min}$ ) exceeds 0.2-inches. If  $L_{min}$  falls below 0.2-inches, there is a deformation (applied- $J$ ) dependent value of  $L_{min}$  below which reasonably accurate  $J_{SSY}$  estimation is possible. At higher levels of overmatch (50% to 100%), it is no longer possible to parameterize departure of  $J_{SSY}$  for a weldment from that for a homogeneous SE(B) based on  $L_{min}$  alone. Weld geometry significantly influences the accuracy with which  $J_{SSY}$  for a welded SE(B) can be approximated by  $J_{SSY}$  for a homogeneous specimen at these extreme overmatch levels.

## 7. REFERENCES

- [1] Hutchinson, J.W., "Singular Behavior at the End of a Tensile Crack in a Hardening Material," *Journal of Mechanics and Physics of Solids*, Vol. 16, pp. 13–31, 1986.
- [2] Rice, J.R., and Rosengren, G.F., "Plane Strain Deformation Near a Crack Tip in a Power-Law Hardening Material," *Journal of Mechanics and Physics of Solids*, Vol. 16, pp. 1–12, 1968.
- [3] Sumpter, J.D.G., "Prediction of Critical Crack Size in Plastically Strained Welded Panels," *Non-linear Fracture Mechanics: Volume II – Elastic-Plastic Fracture*, ASTM STP 995, J.D. Landes, A. Saxena, and J.G. Merkle, Eds., American Society for Testing and Materials, Philadelphia, PA, pp.415–432, 1989.
- [4] Kirk, M.T., and Dodds, R.H., "An Analytical and Experimental Comparison of  $J_i$  Values for Shallow Through and Part Through Surface Cracks," *Engineering Fracture Mechanics*, Vol. 39, No. 3, pp. 535–551, 1991.
- [5] Sorem, W.A., Dodds, R.H., and Rolfe, S.T., "Effects of Crack Depth on Elastic Plastic Fracture Toughness," *International Journal of Fracture*, Vol. 47, pp. 105–126, 1991.
- [6] Kirk, M.T., Koppenhoeffler, K.C., and Shih, C.F., "Effect of Constraint on Specimen Dimensions Needed to Obtain Structurally Relevant Toughness Measures," to appear in the proceedings of the ASTM conference on *Constraint Effects in Fracture* held in Indianapolis, Indiana, May 1991.
- [7] Dodds, R.H., Anderson, T.L., and Kirk, M.T., "A Framework to Correlate  $a/W$  Ratio Effects on Elastic-Plastic Fracture Toughness ( $J_c$ )," *International Journal of Fracture*, Vol. 48, pp. 1–22, 1991.

- [8] Keeney–Walker, J., Bass, B.R., and Landes, J.D., “An Investigation of Crack Tip Stress–Field Criteria for Predicting Cleavage Crack Initiation,” to appear in ASTM STP 1131.
- [9] Anderson, T.L., and Dodds, R.H., “Specimen Size Requirements for Fracture Toughness Testing in the Ductile–Brittle Transition Region,” *Journal of Testing and Evaluation*, Vol. 19, pp. 123–134, 1991.
- [10] Ritchie, R.O., Knott, J.F., and Rice, J.R., *Journal of the Mechanics and Physics of Solids*, Vol. 21, pp. 395–410, 1973.
- [11] Rice, J.R., and Tracey, D.M., in *Numerical and Computer Methods in Structural Mechanics*, S.J. Fenves et al. (eds.), Academic Press, New York, pp.585–623, 1968.
- [12] McMeeking, R.M., *Journal of the Mechanics and Physics of Solids*, Vol. 25, pp. 357–381, 1977.
- [13] McMeeking, R.M., and Parks, D.M., *Elastic–Plastic Fracture*, ASTM STP 668, American Society for Testing and Materials, Philadelphia, PA, pp.175–194, 1979.
- [14] Miglin, M.T., Wade, C.S., and Van Der Sluys, W.A., “Analysis of Fracture Toughness Data for Modified SA508 C12 in the Ductile–to–Brittle Transition Region,” *Fracture Mechanics: Twenty–First Symposium*, ASTM STP 1074, J.P. Gudas, J.A. Joyce, and E.M. Hackett, Eds., American Society for Testing and Materials, Philadelphia, PA, pp.238–263, 1990.
- [15] Herrens, J., and Read, D.T., “Fracture Behavior of a Pressure Vessel Steel in the Ductile–to–Brittle Transition Region,” NISTIR 88–3099, National Institute for Standards and Technology, Boulder, Colorado, December, 1988.
- [16] Barsom, J.M., and Rolfe, S.T., *Fracture and Fatigue Control in Structures – Applications of Fracture Mechanics*, p. 265, 1987.
- [17] Dodds, R.H., and Lopez, L.A., “Software Virtual Machines for Development of Finite Element Systems,” *International Journal for Engineering with Computers*, Vol. 13, pp. 18–26, 1985.
- [18] Li, F.Z., Shih, C.F., and Needleman, A., “A Comparison of Methods for Calculating Energy Release Rates,” *Engineering Fracture Mechanics*, Vol. 21, pp. 405–421, 1985.
- [19] Shih, C.F., Moran, B., and Nakamura, T., “Energy Release Rate Along a Three–Dimensional Crack Front in a Thermally Stressed Body,” *International Journal of Fracture*, Vol. 30, pp. 79–102, 1986.
- [20] Kirk, M.T., and Dodds, R.H., Jr., “Experimental  $J$  Estimation Formulas for Single Edge Notch Bend Specimens Containing Mismatched Welds,” University of Illinois, Urbana, Illinois, Structural Research Series Report SRS–564, December 1991.